agronomy

MDPI

Article

Methodology for Olive Pruning Windrow Assessment Using 3D Time-of-Flight Camera

Francisco J. Castillo-Ruiz [1,2,*], Jose T. Colmenero-Martinez [1], Sergio Bayano-Tejero [1], Emilio J. Gonzalez-Sanchez [1], Francisco M. Lara [1] and Gregorio L. Blanco-Roldán [1]

[1] Department of Rural Engineering, E.T.S.I. Agronomos y Montes, University of Cordoba, Campus de Rabanales, Ctra. N IV Km 396, 14014 Cordoba, Spain; g32comaj@uco.es (J.T.C.-M.); p52bates@uco.es (S.B.-T.); emilio.gonzalez@uco.es (E.J.G.-S.); o22larif@uco.es (F.M.L.); ir3blrog@uco.es (G.L.B.-R.)

[2] Department of Agriculture and Food, Faculty of Science and Technology, University of La Rioja, C/Madre de Dios 53, 26006 Logroño, Spain

* Correspondence: francisco-jose.castillo@unirioja.es; Tel.: +34-94-129-9735

Abstract: The management of olive pruning residue has shifted from burning to shredding, laying residues on soil, or harvesting residues for use as a derivative. The objective of this research is to develop, test, and validate a methodology to measure the dimensions, outline, and bulk volume of pruning residue windrows in olive orchards using both a manual and a 3D Time-of-Flight (ToF) camera. Trees were pruned using trunk shaker targeted pruning, from which two different branch sizes were selected to build two separate windrow treatments with the same pruning residue dose. Four windrows were built for each treatment, and four sampling points were selected along each windrow to take measurements using both manual and 3D ToF measurements. Windrow section outline could be defined using a polynomial or a triangular function, although manual measurement required processing with a polynomial function, especially for high windrow volumes. Different branch sizes provided to be significant differences for polynomial function coefficients, while no significant differences were found for windrow width. Bigger branches provided less bulk volume, which implied that these branches formed less porous windrows that smaller ones. Finally, manual and 3D ToF camera measurements were validated, giving an adequate performance for olive pruning residue windrow in-field assessment.

Keywords: biomass; mulching; bulk volume; windrow outline; windrow shape; shredding; chopping; grinding

Citation: Castillo-Ruiz, F.J.; Colmenero-Martinez, J.T.; Bayano-Tejero, S.; Gonzalez-Sanchez, E.J.; Lara, F.M.; Blanco-Roldán, G.L. Methodology for Olive Pruning Windrow Assessment Using 3D Time-of-Flight Camera. *Agronomy* **2021**, *11*, 1209. https://doi.org/10.3390/agronomy11061209

Academic Editor: Giovanni Caruso

Received: 27 April 2021
Accepted: 11 June 2021
Published: 14 June 2021

1. Introduction

The world's olive growing surface area experienced continuous growth and had reached 11.7 Mha, but by 2019 it had decreased to 11.5 Mha [1]. Europe is home to 55% of the world's olive surface, with more than 2.6 Mha in Spain, among the other main producing countries that are located in the Mediterranean basin [2]. Keeping the olive sector competitive and profitable is therefore an important issue, considering the outstanding importance of olive growing for the economy and creation of employment [3] in large rural areas. Owing to the sector's relevance, Innolivar carries out public pre-commercial procurement to improve the competitiveness of the olive sector through innovation in mechanization, sustainability, olive oil quality, and biotechnology [4]. Within this project, one line of innovation is the commitment to improving the management of olive pruning residue and developing an integral device for windrowing, shredding, and managing traditional and intensive olive pruning residue. This residue could be harvested as biomass or spread on the ground as mulch.

As a source of biomass, olive pruning could provide between 2.5 t ha^{-1} and 14 t ha^{-1} of pruning fresh weight in multi-trunk traditional olive orchards [5] and traditional big-sized trees [6], respectively. Other orchard categories could provide different values of pruning residue for biomass production, oscillating between 1 and 10 t ha^{-1} for super-high density olive orchards [7], while high-density orchards produce 1.2 to 18.5 t ha^{-1} [8]. Furthermore, for the olive crop, pruning biomass production is highly variable depending on several agronomical factors such as the cultivar, pruning frequency [9], pruning system, soil fertility, or availability of water. Pruning waste could be burned in the field, shredded for use as a mulch to protect soil against erosion or increase soil organic matter content, or even harvested for energetic or other productive purposes. Farmers have stopped burning pruning residue and started shredding it, mainly motivated by narrower tree spacing and the consequent tree damage, but also due to local legal restrictions on burning aimed at preventing wildfires [10].

Currently, there is an increase in the shredding of olive pruning residue, which contributes to an improved life-cycle assessment for the carbon footprint related with olive oil [11], which could be used as a green marketing tool [12]. Pruning residues are usually used as mulching to mitigate soil erosion and improve soil fertility [13]. These pruning residue management strategies are boosted within each country or region by specific legal restrictions on groves near forestry areas [14], or by cost-saving strategies that have extended pruning residue shredding based on interactions between farmers [15]. Furthermore, environmental data could be included in an olive traceability system to give carbon fixation or circular economy data that would be highly valued by consumers [16].

Recycling pruned orchard materials and other derivatives could improve olive orchard sustainability [17]. For instance, waste valorization should be considered as a transition phase towards a circular waste-based bio-economy and implemented as part of an integral approach [18]. Olive pruning residues could be valorized by means of different initiatives such as for energetic purposes [19] covering an important part of pellet consumption [20] or processing olive pruning in biorefineries. In these facilities, olive pruning could be processed along with olive leaves and pomace [21] as these residues are a potential source of natural antioxidants [22] or could be used to extract cellulose nanofibers [23]. However, such processes require assessment and development from sociological, biological, and chemical perspectives [24], while for energetic uses, biomass energy policy tools and local initiatives need strengthening to increase biomass consumption in district heating systems [25].

Despite biomass harvesting providing a net gain in the economic and energetic balance, careful operational planning is needed to keep harvesting costs within acceptable values [26]. Nonetheless, pruning shredders by themselves usually have high power requirements, from 50 to 150 kW [27], as well as high human labor requirements, mainly for pruning residue windrowing, which consists of gathering the pruned branches to build a windrow. A windrow is a row of pruned branches built manually or mechanically with the help of mechanical rakes, which reduce operation time compared to manual windrowing [28]. This operation has great importance considering that it must adapt to the shredder, particularly in terms of windrow width, which should match the shredder's working width in order to avoid biomass loss during the harvesting operation [6] or machine feeders missing out branches.

The objective of this study is to develop, test, and validate a methodology to measure the dimensions, outline and bulk volume of pruning residue windrows in olive orchards. Validation of this methodology used both manual and 3D Time-of-Flight (ToF) camera measurements. The article also discusses possible uses for this technology.

2. Materials and Methods

Field tests were conducted in a multi-trunk traditional olive (*Olea europaea* L.) orchard in southern Spain (37.901° N, 4.621° W), planted with the cultivar. Trees had two to three trained trunks, with pruning every two years. The pruned branches obtained during the

2017 pruning season were used to build pruning residue windrows for subsequent shredding. Trees had a spacing of 10 × 10 m, managed under regulated deficit irrigation.

Trees were pruned using trunk shaker targeted pruning [5], branches were separated into five categories according to fresh weight, previous canopy position and cut diameter. Branch fresh weight included wood, leaves, and twigs. Branch categories were defined during this and previous tests in the same orchard from 2013, although we only used two of the categories for the current research (Figure 1):

- Scaffold limbs: Branches adjoined to a tree trunk with a cut diameter over 0.12 m and fresh weight higher than 25 kg branch^{-1}.
- Secondary branches: These branches usually adjoin scaffold limbs, have a cut diameter between 0.12 and 0.06 m and a fresh weight between 25 and 5 kg branch^{-1}.
- Third branches: They could adjoin both scaffold limbs and secondary branches, and had a cut diameter between 0.06 and 0.03 m. For this branch category, fresh weight was between 5 and 1 kg branch^{-1}.
- Supporting bearing branches: these branches supported the fruit-bearing branches, had a cut diameter between 0.03 and 0.015 m, and a fresh weight between 1 and 0.3 kg branch^{-1}.
- Bearing branches: The fruit bearing branches, with very little wood, a cut diameter under 0.015 m, and a fresh weight lower than 0.3 kg branch^{-1}.

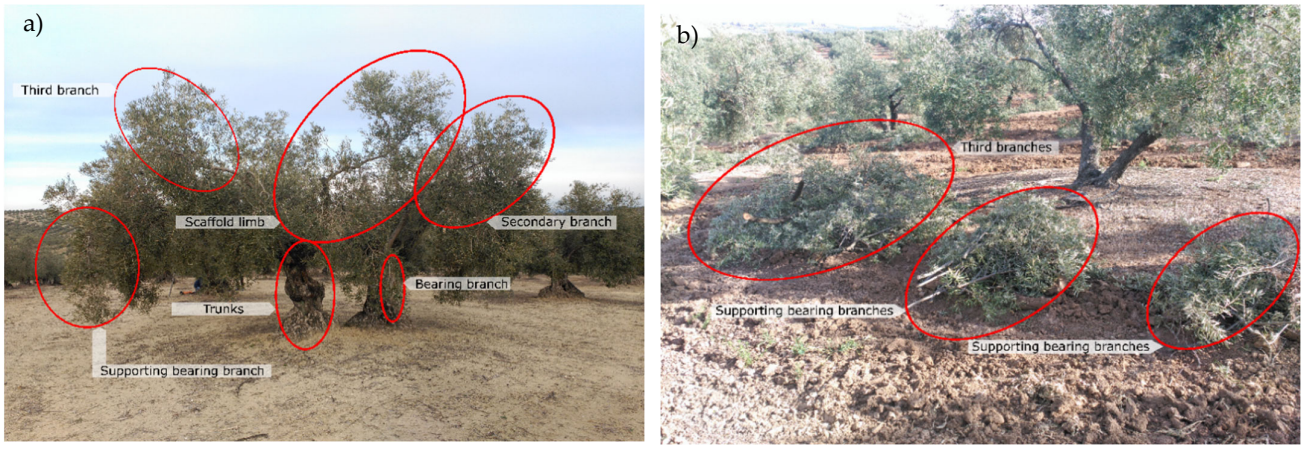

Figure 1. The five branch categories, shown on a traditional multi-trunk tree before pruning (**a**) and during branch classification before building the pruning windrows (**b**).

Two treatments were applied to build a pruning residue windrow with two different groups of branch sizes: third branches and supporting bearing branches. We did not consider other branch categories because the bigger branches had previously been chopped, removing firewood, and bearing branches had little influence on the shredding process or on windrow features. Four, 20 m-long windrow replications were used for both treatments, maintaining a constant amount of pruning residue at 2.65 kg m^{-1} along the whole windrow (Figure 2). To keep the amount of pruning residue constant, the same number of branches were placed per meter to ensure, as much as possible, a constant dose of pruning residues (Table 1).

Table 1. The two treatments applied to build windrows using different branch categories depending on fresh weight, cut diameter, and pruning residue amount.

Value	Third Branches	Supporting Bearing Branches
Fresh weight (kg branch^{-1})	2.79 ± 1.03	0.52 ± 0.16
Cut diameter (mm)	34.38 ± 6.23	18.34 ± 4.3
Pruning residue amount (kg fresh weight m^{-2})	2.9 ± 1.0	2.8 ± 0.6
Pruning residue amount (branches m^{-1})	3 ± 1	15 ± 3
Replications per treatment	4	4
Length of each windrow replication (m)	20	20
Measurements per replication	4	4

Figure 2. Windrow replication of 20 m length before shredding. Branches were placed transversally to the tractor's forward direction, leaving trunks in the center of the windrow.

We measured windrow width and height in the center of the transversal section manually. Alternatively, other measurements were taken using a 3D Time-of-Flight (ToF) camera (IFM electronic, Essen, Germany), with an infrared illumination unit (IFM, O3M950) and 3D sensor (IFM, O3M151). The 3D ToF camera had an aperture angle of 70 × 23 º, which were oriented to Y- and Z-axes, respectively. An aluminum supporting structure for in-field measurements was built to hold the illumination unit and sensor in zenith position over the pruning residue windrow. This structure held the illumination unit and sensor 3.37 m above the soil. The sensor field of vision was constricted to 4.3 m along the cross-windrow axis (Y-axis) and 1.3 m along the lengthwise-windrow axis (Z-axis). The field of vision was divided into 64 regions of interest (ROIs), which were prisms uniformly distributed in 4 rows and 16 columns. This was considered sufficient to encompass the

whole windrow width. Each ROI determined one voxel including 16 measurements (pixels), of which the nearest was selected as the voxel height. Therefore, the 3D ToF camera measured the highest point within each ROI, considering that the camera measured the shortest distance to the sensor. Thus, pruning-residue bulk volume was measured for each ROI. To calculate the total section bulk volume, all measured ROI bulk volumes were summed, using each ROI height (h_{ROI}) and voxel base (Table 2) (1).

Table 2. 3D ToF camera calibration values. ROI: Region of interest.

Axis	Minimum (m)	Maximum (m)	Voxel Size (ROI) (m)	Direction
X	0	3.37	3.37	Lengthwise-windrow axis
Y	−2.15	2.15	0.26875	Cross-windrow axis
Z	2.70	4	0.325	Vertical

$$Bulk\ volume_{ROI}\ (m^3) = \sum_{64}^{i=1}(0.26875 \times 0.325 \cdot h_{ROI_i}) \quad (1)$$

The statistical design consisted of considering each windrow replication as a block and taking four measurements along each windrow for both manual and camera methodologies. The 3D ToF camera measurements were used to determine windrow shape for both third branches and supporting bearing branches. For this purpose, all 3D ToF camera measurements were represented to build a regression; however, due to the windrow's shape, measurements need transformation to adjust to a linear function and describe the whole windrow. Due this fact, x values were modified by applying a symmetry function (2) into x′ values, which were only used to apply straight regressions to determine windrow shape. The resulting function should be considered half of the whole windrow for calculation of the whole windrow section. All regression equations were forced to pass through the point (0, 0) because at this point, the windrow height should be 0 m.

$$x' = |x - 2.15| + 2.15 \quad (2)$$

3. Results

Firstly, we determined the shape of the pruning-residue windrow section using the height measurements of each sampled cross-section, which provided 4 rows of 16 ROIs on the windrow cross-section axis. The Y and Z 3D ToF camera axes (Table 2) were taken to plot windrow shape graphs. Cross ROI position varied, depending on the location of the highest point of each ROI, providing an almost continuous cloud of points to define windrow shape. The transversal profile of the windrow was adjusted to a polynomial or triangular shape, obtaining similar results in both cases (Figure 3). It is important to consider that when the windrow was supposed to have a triangular shape, regression only showed half of the windrow section, considering that a symmetry function had previously been applied to transform measured points (2).

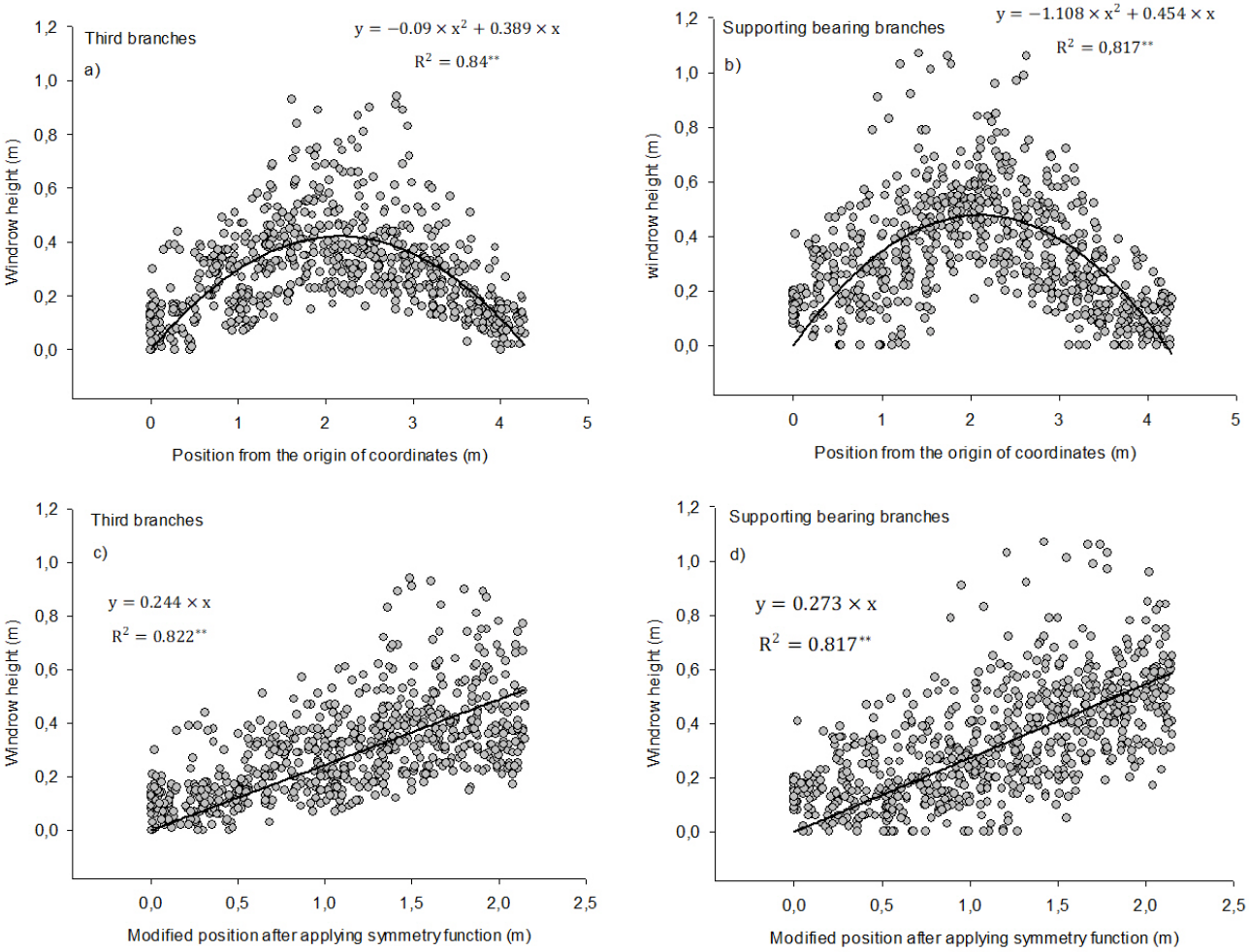

Figure 3. Transversal profile regression functions for the measured windrows using a polynomial function for third branches (a) and supporting bearing branches (b). In addition, windrow shape was transformed into a linear regression to represent triangular-shaped sections for third branches (c) and supporting bearing branches (d). Significance level indicated by ** ($p < 0.01$). Windrow height was represented by y (vertical axis) and R was coefficient of determination.

Despite the 3D ToF camera's accuracy, we intended to develop a simplified method to enable the quick measurement of windrow bulk volume using a manual method. This manual method could become an automatic measurement using cheap and simple sensors installed on shredding machines. To achieve the development of this method, we measured height in the middle of the windrow cross axis (h) and windrow width along the cross section (w). Applying a polynomial windrow shape, a system of linear equations was established to estimate windrow shape based on these manual measurements, calculating a and b coefficients separately for each branch size windrow (Table 3) (3).

$$\begin{aligned} h &= a \times \left({}^{w}/_{2}\right)^{2} + b \times w \\ 0 &= a \times w^{2} + b \times w \end{aligned} \quad (3)$$

Table 3. Coefficients and windrow dimensions calculated for manual measurements of pruning windrows depending on branch size. Signification column calculated according to Student's test. NS (No significant) $p > 0.05$; * $p < 0.05$; ** $p < 0.01$.

Coefficient/value	Third branches	Supporting bearing branches	Significance
a	−0.38 ± 0.15	−0.53 ± 0.21	0.049*
b	1.02 ± 0.30	1.40 ± 0.40	0.016*
Windrow maximum height (m)	0.72 ± 0.15	0.94 ± 0.20	0.006**
Windrow width (m)	2.93 ± 0.62	2.75 ± 0.37	0.408^{NS}

Third branches and supporting bearing branches provide different coefficients for a polynomial fitting (Table 3), but both branch sizes were adjusted to a polynomial shape in the form $y = ax^2 + bx$ (Figure 3). Therefore, it was possible to calculate the equation that determined the shape of the windrow for each sampling point by integrating this polynomial function within width limits. A windrow was considered as centered with respect to the Y-axis for calculation of the mean windrow section using a polynomial fitting (4.3 m) (4). Figure 3 shows that it was also possible to define windrow shape by a triangular function, after applying an inverse symmetry function to previously transformed data. Thus, it was possible to calculate the mean windrow section using maximum height and width (5).

$$Mean\ windrow\ section\ (polynomial) = \int_{(4.3-w)/2}^{(4.3+w)/2} ax^2 + bx \times dx \quad (4)$$

$$Mean\ windrow\ section\ (triangular) = \frac{wh}{2} \quad (5)$$

The manual method for windrow bulk volume measurement was validated based on 3D ToF camera measurements, providing a highly significant correlation ($R^2 = 0.691$; $p < 0.01$), which indicated that, despite showing differences for absolute values (Table 4), manual measurements were suitable to determine windrow bulk volume. It should be highlighted that windrow bulk volume, calculated by manual measurements using triangular fitting, underestimated real windrow bulk volume compared to the camera bulk volume. Moreover, the greater the windrow bulk volume, the higher the deviation of manual bulk volume using triangular fitting, as the validation models show. Therefore, calculation of windrow shape using manual measurements should use polynomial fitting rather than triangular fitting to avoid high deviation at high windrow volumes (Figure 4).

Table 4. Windrow bulk volumes and section for the different calculation processes and treatments.

Branch Size	Third Branches			Supporting Bearing Branches		
Calculation process	Camera	Manual triangular	Manual Polynomial	Camera	Manual triangular	Manual Polynomial
Measured bulk volume (m^3)	1.75 ± 0.48	1.36 ± 0.38	1.82 ± 0.51	1.96 ± 0.54	1.68 ± 0.39	2.23 ± 0.52
Mean windrow section (m^2)	1.35 ± 0.37	1.05 ± 0.29	1.40 ± 0.39	1.51 ± 0.42	1.29 ±0.3	1.72 ± 0.40
Pruning residue amount (branches m^{-1})		3 ± 1			15 ± 3	
Pruning residue amount (kg fresh weight m^{-2})		2.9 ± 1.0			2.8 ± 0.6	

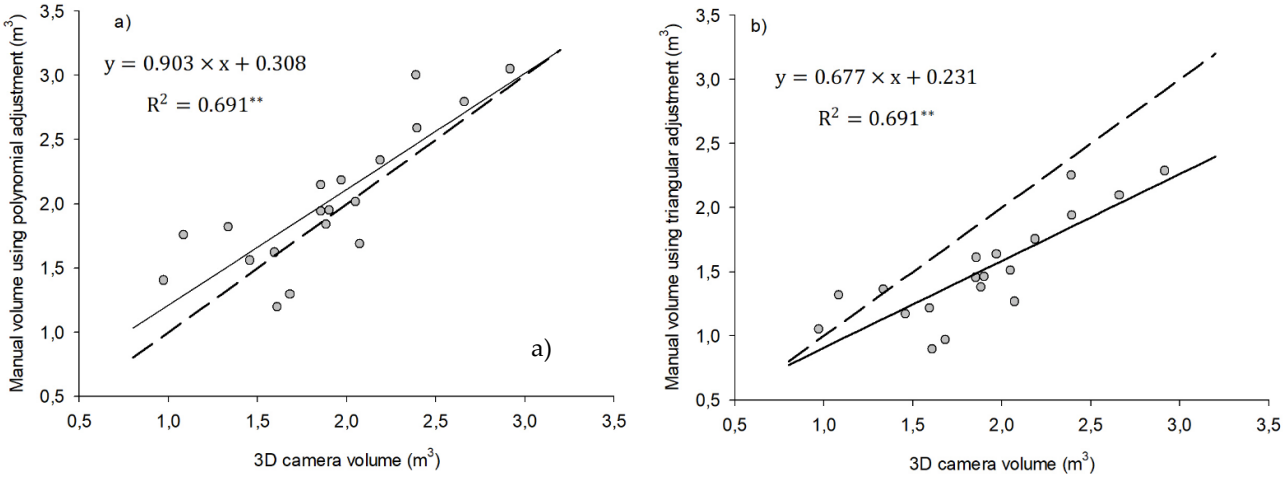

Figure 4. Validation of manual bulk volume based on camera bulk volume for manual polynomial fitting (**a**) and for manual triangular fitting (**b**). Solid lines define linear regression, while dashed lines define y=x function. Significance level indicated by ** ($p < 0.01$). Vertical axis was represented by y and R was coefficient of determination.

4. Discussion

Manual and 3D ToF camera measurements provided similar windrow bulk volume, providing a similar windrow height. Both methods also coincided in windrow width measurements; however, windrow width was almost twofold in these tests compared with other tests performed in Italy, whereas windrow height was only slightly higher [6]. Differences in windrow dimensions were not justified based on pruning residue fresh weight, which varied between 8.4 ± 2.8 t ha^{-1} for third branches and 7.8 ± 1.6 t ha^{-1} for supporting bearing branches, while in the Italian tests it was 14 t ha^{-1}. Nonetheless, the absence of a relationship between pruning residue amount and windrow dimensions could be due to differences in the way branches are laid on the windrow. This fact could also be due to the windrowing method employed, which may cause differences between mechanical and manual windrowed branches. Moreover, for manually built windrows, it should be considered that operating time for this task increases when the windrow is narrower [27]. It could be hypothesized that branch size may influence windrow size, but in

our research, this fact only significantly affected windrow height, whereas windrow width was independent of branch size. Supporting bearing branches provided higher windrows than third bearing branches, which could be due to higher windrow porosity when branch size is smaller. Furthermore, windrow shape depended on branch size, providing different coefficients for each treatment (Table 3).

The 3D ToF camera measurements provided a reliable and highly accurate method to determine windrow bulk volume. However, an important consideration is that completing one section measurement with the 3D ToF camera takes 4–6 min per measured point (to establish the supporting structure, straighten the camera and take measurements), whereas manual measurements provide a faster method to measure windrow bulk volume. In addition, it is important to highlight that post-field data processing required further time to calculate the windrow section with the 3D ToF camera. Considering that the amount of pruning residue was similar, the windrow bulk volume of supporting bearing branches was significantly higher ($p > 0.05$ according to Student's T test). This fact confirmed that smaller branches provided windrows that are more porous, which could affect some machine parameters such as the feeding system dimensions, power requirements, or the amount of biomass harvested. Furthermore, other factors may influence power requirements, such as the type of hammers or blades [29], pruning residue moisture, the cross-sectional area of the wood, or the cultivar [30]. Once pruning residues were shredded, biomass logistics was a key factor. The density of chipped material determined transport requirements, although other methods could be used to increase biomass density, such as baling [31].

Further research should develop uses for windrow bulk volume and dimensions to acquire data or to automatize shredding of windrowing operations such as pruning residue feeding system adjustments. The manual measurements used to determine windrow bulk volume were validated based on the 3D ToF camera (Figure 4), which could be substituted by other automatic technologies capable of measuring windrow dimensions such as a laser scanner [32], ultrasonic sensors [33], or LIDAR [34] to calculate windrow bulk volume supposing a polynomial windrow shape (Table 4; Figure 4). Other research has compared UAV-based technologies and RGB-D reconstruction methods to estimate biomass height and dry biomass in pastures, describing how an on-ground RGB-D system provides more accurate results [35]. Such systems might be highly useful to control machine feeding and shredding systems by continuous measurement of windrow height and width alone, and to optimize shredding power requirements. Windrow bulk volume could constitute a quick method to evaluate the harvested amount of tree pruning biomass in olive orchards, assessing the influence of branch size on windrow bulk volume and porosity. Pruning residue linear density along the windrow also influences operating time, although biomass harvesting productivity is directly proportional to linear density [36], which may justify concentrating residue on alternate inter-rows [8]. However, this strategy would make branch windrowing more difficult for both manual and mechanical procedures. Olive pruning residue windrowing slows down subsequent shredding operations. Furthermore, the use of mechanical windrowers improves the energy balance of the biomass harvesting operation, increasing energy outputs to a greater extent than energy inputs, also improving the profitability of pruning residue harvesting [37].

5. Conclusions

We developed, tested, and validated two methods to measure windrow bulk volume: one method based on 3D ToF camera zenithal measurements and the other on quick and simple manual measurements processed through polynomial fitting. It was determined that windrow shape could be described as either a polynomial function or a triangular function. However, manual measurements require processing with polynomial fitting to reduce errors. Furthermore, it was demonstrated that for the same amount of pruning residue, bigger branches provided less bulk volume, which implied that the branches formed less porous windrows. For this reason, branch size should be controlled to give an

accurate estimation of biomass production by windrow bulk volume measurements. Further research could tackle the installation of sensors on pruning shredders and control of machine variables by adapting the machine to windrow features. Such machine adaption to working conditions is of great importance when shredder power requirements are close to the maximum power of the tractor. Nevertheless, in-field windrowing for commercial orchards results in mixing of branch sizes, which should be evaluated to fit bulk volume calculation in each case.

Author Contributions: Conceptualization, F.J.C.-R.; Data curation, J.T.C.-M.; Formal analysis, F.J.C.-R.; Funding acquisition, G.L.B.-R.; Methodology, F.J.C.-R. and J.T.C.-M.; Project administration, G.L.B.-R.; Resources, S.B.-T.; Supervision, S.B.-T. and E.J.G.-S.; Validation, F.J.C.-R.; Writing—original draft, F.J.C.-R.; Writing—review and editing, J.T.C.-M. and F.M.L. All authors have read and agreed to the published version of the manuscript.

Funding: This research, including APC, was funded through the public pre-commercial procurement agreement Innolivar[1] of the Spanish Ministry of Science, Innovation and Universities along with the support of the Spanish Olive Oil Interprofessional Organization (https://www.aceitesdeolivadeespana.com/).[1]Public procurement of innovative solutions specifically pre-commercial procurement Innolivar according to the agreement signed by before Ministry of Economy, Industry and Competitiveness (current Ministry of Science, Innovation and Universities) and University of Cordoba co-funded by ERDF funds (80%) within multiregional operational program of Spain 2014-2020.

Institutional Review Board Statement: Not applicable.

Informed Consent Statement: Not applicable.

Data Availability Statement: Data sharing not applicable.

Acknowledgments: Authors wish to acknowledge the collaboration of Diego Barranco, who lent his olive orchard and machinery to perform the tests.

Conflicts of Interest: The authors declare no conflict of interest. Moreover, the funders had no role in the design of the study; in the collection, analyses, or interpretation of data; in the writing of the manuscript, or in the decision to publish the results.

References

1. Análisis del olivar a nivel mundial. Available online: https://www.interempresas.net/Grandes-cultivos/Articulos/302096-Analisis-del-olivar-a-nivel-mundial.html (accessed on 17 October, 2020).
2. Agricultural Production—Orchards. Available online: https://ec.europa.eu/eurostat/statistics-explained/index.php/Agricultural_production_-_orchards#Apple_trees (accessed on 18 February 2020).
3. Aceite de oliva. Available online: http://www.mapama.gob.es/es/agricultura/temas/producciones-agricolas/aceite-oliva-y-aceituna-mesa/aceite.aspx#para1 (accessed on Oct 17, 2020).
4. Innolivar Lineas de Convenio. Available online: https://innolivar.es/ (accessed on 17 October 2020).
5. Castillo-Ruiz, F.; Sola-Guirado, R.; Castro-Garcia, S.; Gonzalez-Sanchez, E.; Colmenero-Martinez, J.; Blanco-Roldán, G. Pruning systems to adapt traditional olive orchards to new integral harvesters. *Sci. Hortic.* **2017**, *220*, 122–129, doi:10.1016/j.scienta.2017.03.043.
6. Acampora, A.; Croce, S.; Assirelli, A.; Del Giudice, A.; Spinelli, R.; Suardi, A.; Pari, L. Product contamination and harvesting losses from mechanized recovery of olive tree pruning residues for energy use. *Renew. Energy* **2013**, *53*, 350–353, doi:10.1016/j.renene.2012.12.009.
7. Vivaldi, G.A.; Strippoli, G.; Pascuzzi, S.; Stellacci, A.; Camposeo, S. Olive genotypes cultivated in an adult high-density orchard respond differently to canopy restraining by mechanical and manual pruning. *Sci. Hortic.* **2015**, *192*, 391–399, doi:10.1016/j.scienta.2015.06.004.
8. Spinelli, R.; Picchi, G. Industrial harvesting of olive tree pruning residue for energy biomass. *Bioresour. Technol.* **2010**, *101*, 730–735, doi:10.1016/j.biortech.2009.08.039.
9. Marti, B.V.; Fernández-González, E.; Cortés, I.L.; Salazar-Hernández, D. Quantification of the residual biomass obtained from pruning of vineyards in Mediterranean area. *Biomass- Bioenergy* **2011**, *35*, 3453–3464, doi:10.1016/j.biombioe.2011.04.009.
10. Benyei, P.; Cohen, M.; Gresillon, E.; Angles, S.; Araque-Jiménez, E.; Alonso-Roldán, M.; Espadas-Tormo, I. Pruning waste management and climate change in Sierra Mágina's olive groves (Andalusia, Spain). *Reg. Environ. Chang.* **2018**, *18*, 595–605, doi:10.1007/s10113-017-1230-5.
11. Proietti, S.; Sdringola, P.; Regni, L.; Evangelisti, N.; Brunori, A.; Ilarioni, L.; Nasini, L.; Proietti, P. Extra Virgin Olive oil as carbon negative product: Experimental analysis and validation of results. *J. Clean. Prod.* **2017**, *166*, 550–562, doi:10.1016/j.jclepro.2017.07.230.

12. Iraldo, F.; Testa, F.; Bartolozzi, I. An application of Life Cycle Assessment (LCA) as a green marketing tool for agricultural products: the case of extra-virgin olive oil in Val di Cornia, Italy. *J. Environ. Plan. Manag.* **2013**, *57*, 78–103, doi:10.1080/09640568.2012.735991.
13. Repullo, M.; Carbonell-Bojollo, R.; Hidalgo, J.; Rodríguez-Lizana, A.; Ordóñez, R. Using olive pruning residues to cover soil and improve fertility. *Soil Tillage Res.* **2012**, *124*, 36–46, doi:10.1016/j.still.2012.04.003.
14. Decree 371/2010, de 14 de septiembre, por el que se aprueba el Plan de Emergencia por Incendios Forestales de Andalucía y se modifica el Reglamento de Prevención y Lucha contra los Incendios Forestales aprobado por el Decreto 247/2001, de 13 de noviembre. Available online: http://www.juntadeandalucia.es/boja/2010/192/1 (accessed on 17 October 2020).
15. Calatrava, J.; Franco, J.A. Using pruning residues as mulch: Analysis of its adoption and process of diffusion in Southern Spain olive orchards. *J. Environ. Manag.* **2011**, *92*, 620–629, doi:10.1016/j.jenvman.2010.09.023.
16. Bayano-Tejero, S.; Sola-Guirado, R.R.; Gil-Ribes, J.A.; Blanco-Roldán, G.L. Machine to machine connections for integral management of the olive production. *Comput. Electron. Agric.* **2019**, *166*, 104980, doi:10.1016/j.compag.2019.104980.
17. Zipori, I.; Erel, R.; Yermiyahu, U.; Ben-Gal, A.; Dag, A. Sustainable Management of Olive Orchard Nutrition: A Review. *Agric.* **2020**, *10*, 11, doi:10.3390/agriculture10010011.
18. Zabaniotou, A. Redesigning a bioenergy sector in EU in the transition to circular waste-based Bioeconomy-A multidisciplinary review. *J. Clean. Prod.* **2018**, *177*, 197–206, doi:10.1016/j.jclepro.2017.12.172.
19. Vourdoubas, J. Effect of Soil Moisture Stress Duration on the Growth Characteristics and Yield of Rice Cultivars. *J. Agric. Environ. Sci.* **2016**, *4*, 77–86,, doi:10.15640/jaes.v4n2a9.
20. Soltero, V.M.; Román, L.; Peralta, M.E.; Chacartegui, R. Sustainable biomass pellets using trunk wood from olive groves at the end of their life cycle. *Energy Rep.* **2020**, *6*, 2627–2640, doi:10.1016/j.egyr.2020.09.017.
21. Manzanares, P.; Ruiz, E.; Ballesteros, M.; Negro, M.J.; Gallego, F.J.; López-Linares, J.C.; Castro, E. Residual biomass potential in olive tree cultivation and olive oil industry in Spain: valorization proposal in a biorefinery context. *Span. J. Agric. Res.* **2017**, *15*, e0206, doi:10.5424/sjar/2017153-10868.
22. Martínez-Patiño, J.C.; Gullón, B.; Romero, I.; Ruiz, E.; Brnčić, M.; Žlabur, J. Šic; Castro, E. Optimization of ultrasound-assisted extraction of biomass from olive trees using response surface methodology. *Ultrason. Sonochemistry* **2019**, *51*, 487–495, doi:10.1016/j.ultsonch.2018.05.031.
23. Sánchez-Gutiérrez, M.; Espinosa, E.; Bascón-Villegas, I.; Pérez-Rodríguez, F.; Carrasco, E.; Rodríguez, A. Production of Cellulose Nanofibers from Olive Tree Harvest—A Residue with Wide Applications. *Agron.* **2020**, *10*, 696, doi:10.3390/agronomy10050696.
24. Cohen, M.; Lepesant, G.; Lamari, F.; Bilodeau, C.; Benyei, P.; Angles, S.; Bouillon, J.; Bourrand, K.; Landoulsi, R.; Jaboeuf, D.; et al. Biomolecules from olive pruning waste in Sierra Mágina – Engaging the energy transition by multi-actor and multidisciplinary analyses. *J. Environ. Manag.* **2018**, *216*, 204–213, doi:10.1016/j.jenvman.2017.03.067.
25. Ericsson, K.; Werner, S. The introduction and expansion of biomass use in Swedish district heating systems. *Biomass- Bioenergy* **2016**, *94*, 57–65, doi:10.1016/j.biombioe.2016.08.011.
26. Nati, C.; Boschiero, M.; Picchi, G.; Mastrolonardo, G.; Kelderer, M.; Zerbe, S. Energy performance of a new biomass harvester for recovery of orchard wood wastes as alternative to mulching. *Renew. Energy* **2018**, *124*, 121–128, doi:10.1016/j.renene.2017.07.030.
27. Pari, L.; Suardi, A.; Santangelo, E.; Galindo, D.G.; Scarfone, A.; Alfano, V. Current and innovative technologies for pruning harvesting: A review. *Biomass- Bioenergy* **2017**, *107*, 398–410, doi:10.1016/j.biombioe.2017.09.014.
28. López Giménez, F.J.; Blanco-Roldán, G.L.; Dorado Pérez, M. del P.; Gil-Ribes, J.A. Mecanización de la recogida de restos de poda en olivar: Rendimientos, producciones y costes. *Vida Rural* **2010**, *307*, 46–51.
29. Pari, L.; Suardi, A.; Del Giudice, A.; Scarfone, A.; Santangelo, E. Influence of chipping system on chipper performance and wood chip particle size obtained from peach prunings. *Biomass- Bioenergy* **2018**, *112*, 121–127, doi:10.1016/j.biombioe.2018.01.002.
30. Sessiz, A.; Elicin, A.K.; Esgici, R.; Ozdemir, G.; Nozdrovický, L. Cutting Properties of Olive Sucker. *Acta Technol. Agric.* **2013**, *16*, 82–86, doi:10.2478/ata-2013-0021.
31. Sokhansanj, S.; Webb, E.; Turhollow, A. Cost impacts of producing high density bales during biomass harvest. In Proceedings of the 2014 ASABE Annual International Meeting; American Society of Agricultural and Biological Engineers, EE.UU, 2014; pp. 1–13.
32. Sola-Guirado, R.R.; Bayano-Tejero, S.; Rodríguez-Lizana, A.; Gil-Ribes, J.A.; Miranda-Fuentes, A. Assessment of the Accuracy of a Multi-Beam LED Scanner Sensor for Measuring Olive Canopies. *Sensors* **2018**, *18*, 4406, doi:10.3390/s18124406.
33. Gamarra-Diezma, J.L.; Miranda-Fuentes, A.; Llorens, J.; Cuenca, A.; Blanco-Roldán, G.L.; Lizana, A.R. Testing Accuracy of Long-Range Ultrasonic Sensors for Olive Tree Canopy Measurements. *Sensors* **2015**, *15*, 2902–2919, doi:10.3390/s150202902.
34. Miranda-Fuentes, A.; Llorens, J.; Gamarra-Diezma, J.L.; Gil-Ribes, J.A.; Gil Moya, E. Towards an Optimized Method of Olive Tree Crown Volume Measurement. *Sensors* **2015**, *15*, 3671–3687, doi:10.3390/s150203671.
35. Rueda-Ayala, V.P.; Peña, J.M.; Höglind, M.; Bengochea-Guevara, J.M.; Andújar, D. Comparing UAV-Based Technologies and RGB-D Reconstruction Methods for Plant Height and Biomass Monitoring on Grass Ley. *Sensors* **2019**, *19*, 535, doi:10.3390/s19030535.

36. Spinelli, R.; Nati, C.; Magagnotti, N. Using modified foragers to harvest short-rotation poplar plantations. *Biomass- Bioenergy* **2009**, *33*, 817–821, doi:10.1016/j.biombioe.2009.01.001.
37. Dyjakon, A. The Influence of the Use of Windrowers in Baler Machinery on the Energy Balance during Pruned Biomass Harvesting in the Apple Orchard. *Energies* **2018**, *11*, 3236, doi:10.3390/en11113236.